

3D microfabricated bioreactor with capillaries

Chunguang Xia · Nicholas X. Fang

Published online: 6 October 2009
© Springer Science + Business Media, LLC 2009

Abstract We present in this paper the implementation of an innovative three dimensional (3D) microfabrication technology coupled with numerical simulation to enhance the mass transport in 3D cell culture. The core of this microfabrication technology is a high-resolution projection micro stereolithography (PμSL) using a spatial light modulator as a dynamic mask which enables a parallel fabrication of highly complex 3D microstructures. In this work, a set of poly (ethylene glycol) microfabricated bioreactors are demonstrated with PμSL technology. We observed both experimentally and numerically the regulation of metabolism and the growth of yeast cells by controlling the density of micro-capillaries. Further development of these 3D microfabricated bioreactors is expected to provide artificially constructed tissues for clinical applications.

Keywords 3D microfabrication · Bioreactor · Transport · Modeling · Vascular

1 Introduction

Reconstructive surgeries are performed to recover the function and appearance of damaged tissues, especially following major cancer resections and traumas. It is estimated that more than one million reconstructive surgery procedures are performed by plastic surgeons every year. The development of reconstructive surgery (Dunn and

Watson 2001) has proved the success of free flaps as reconstructive tissues for recipients. A free flap is a block of tissue with inherent microcirculatory network, usually is transferred from a patient's own body close to the defective site (Taylor and Palmer 1987). However, the nature of sacrificing one part of a body for another limits the application of free flaps in practice. Therefore alternative tissue sources for reconstructive surgery are desired. The field of tissue engineering (Berthiaume and Yarmush 2002) introduces the exciting possibility of replacing damaged body parts with new ones customized to the specific needs of the recipient, independent of the availability of donor sources. A number of tissue-engineered products are currently used clinically, such as Integra™, Carticeal™, and Apligraf™. Further development of cell biology, microtechnology, and biomaterial science will provide new opportunities to create larger and more complex artificial tissues.

One of the major obstacles towards the creation of large complex 3D artificial tissues is the lack of microcirculatory system at the early stage of tissue culture (Ruben et al. 2005). The time scale for neo-vascularization is in the order of days (even with growth factors) and the time scale for cell death from hypoxia is in the order of hours. Therefore without capillary perfusion, the metabolism during cell growth cycles will eventually exhaust the supply of nutrient and oxygen from the external environment and the embedded cells suffer from the lack of nourishment, creating a bottleneck for the growth of thick (>1 mm scale) 3D tissues. Studies (Sutherland et al. 1986; Martin et al. 1999) confirmed that cells in a tissue were poorly cultured when they were further than ~400 μm away from external nutrient sources. As a matter of fact, in real tissues, most of cells stay within a distance of about 100 μm from nearby capillaries (Berthiaume and Yarmush 2002). Several re-

C. Xia · N. X. Fang (✉)
Department of Mechanical Science and Engineering,
University of Illinois at Urbana-Champaign,
158 Mechanical Engineering Building, MC-244,
1206 West Green Street,
Urbana, IL 61801-2906, USA
e-mail: nicfang@illinois.edu

search groups have developed methods to enhance the mass transport in tissue culture by taking advantage of current microfabrication technologies. For example, by inserting and extracting nylon strands and tubing, straight artificial blood vessels were created to allow the continuous perfusion of culture medium (Neumann et al. 2003). However, the assembly of many discrete micro blood vessels into an inner-connected 3D network for nutrient perfusion will not be practical. Griffith, et al (Griffith et al. 1997) created 3D channels by 3D printing technology. Unfortunately, the resolution of this technology was only 200 μm , which is much larger than a capillary dimension ($<20 \mu\text{m}$). Silicon microfabrication technologies and molding were also able to create two dimensional micro channels for enhanced mass transport (Borenstein et al. 2002). A recent study (Levenberg et al. 2005) shown a multi-culture system consisting of myoblasts, embryonic fibroblasts and endothelial cells co-seeded on highly porous, biodegradable polymer scaffolds could induce the endothelial vessel networks. However the scaffolds used in this work were less than 1 mm thick, which is still within the diffusion distance of external nutrients. Nevertheless, the three dimensional nutrient transport in thick ($>1 \text{ mm}$) tissue culture still remains a hurdle in tissue engineering.

To enhance the transport and exchange of nutrients and wastes for constructing thick artificial tissues, a novel three dimensional microfabrication technology, projection micro stereolithography (P μ SL) (Sun et al. 2005), is introduced for the design and the fabrication of vascularized micro bioreactors. We show in this work such micro fabricated bioreactors, coupled with mass transport simulation, can dramatically enhance the nutrition and growth of cultured cells through capillary networks. This microfabrication method brings several unique advantages to the field of tissue engineering: first, the capability of P μ SL to build truly 3D sophisticated microstructures with very fine spatial resolution at micron scale; second, a significantly shortened design cycle enabled by high fabrication speed (500 layers in a couple of hours); finally, the choice of biocompatible and biodegradable polymers offers flexibility on fabricating implantable pre-vascularized scaffolds for different tissue cultures (Ratner and Bryant 2004; Hou et al. 2004).

2 Microfabrication and materials

The principle of P μ SL is highlighted in Fig. 1. The process starts by generating a 3D structure using Computer-Aided Design (CAD) software and then slices the structure into a sequence of mask images (digital mask). Each image represents a thin layer (usually 5–30 microns thick) of the 3D structure. During a fabrication cycle, a single image is displayed on the reflective liquid crystal display (LCD)

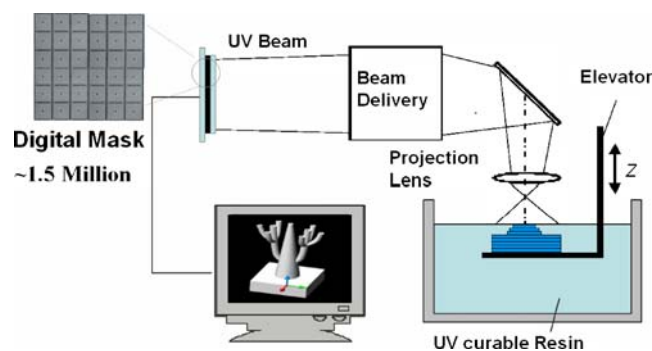


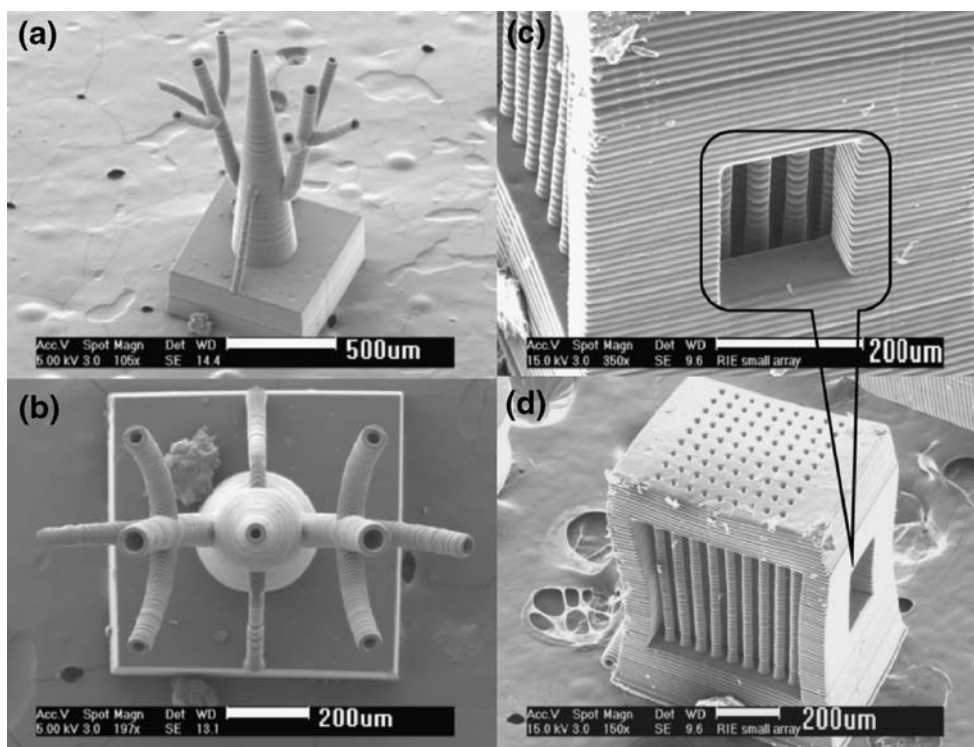
Fig. 1 Projection micro stereolithography system

panel. The image on the LCD is then delivered and projected onto the photo curable liquid surface. The whole layer is polymerized simultaneously. After one layer is solidified, the polymerized component is re-immersed into the resin to allow the formation of a new thin liquid layer on top of it, and a new fabrication cycle starts. By repeating the cycles, a 3D microstructure is formed from a stack of layers.

P μ SL is compatible with various biomaterials of different functions, for example biocompatible and biodegradable polymers including Poly (ethylene glycol) (PEG), poly lactic acid (PLA), poly caprolactone (PCL), and their copolymers. In this work, the monomer is a water-soluble PEG diacrylate (molecular weight 575, from Sigma-Aldrich, with viscosity 57 cP at 25°C). Bis(2,4,6-trimethylbenzoyl)-phenylphosphineoxide (Irgacure 819, from Ciba) is used as the photo initiator. A small amount of UV absorber (0.5–0.8 wt %) is mixed with the PEG monomer to control the UV penetration depth in the solution. Two representative 3D structures are presented in Fig. 2. In Figs 2(a) and (b), we show a highly branched capillary network structure is readily produced in this microfabrication technique; the inner radius of those capillaries vary from 10 μm to 30 μm . Figures 2(c), (d) are different views of a 9 by 9 capillary array with 10- μm inner radius, 20- μm outer radius, 80- μm spacing and 800- μm in length (aspect ratio >20 , effective channel density $>150/\text{mm}^2$). Table 1 summarizes the basic capabilities of our P μ SL system.

Not only is P μ SL capable of constructing 3D complex polymer capillaries with high resolution, it also offers potential of locally controlling the young's modulus (Manias et al. 2001) and permeability of the polymer structures. The cross-linking ratio of photo-curable polymer increases as the exposure dose increases and finally reaches a plateau (Fang et al. 2004). Meanwhile, the permeability of the photo-cured polymer is a function of cross-linking ratio, the permeability decreases as the cross-linking ratio increases (Fig. 3). Therefore, by simply controlling the exposure dose for each layer and within each layer in the fabrication process, the permeability of 3D structures can be precisely, locally tuned in a 3D space. This technology

Fig. 2 High-resolution 3D micro structures fabricated by PμSL



has a great potential application of local delivery in tissue engineering devices.

3 Vascularized micro bioreactor

During a tissue culture, it is very important that all the cells in the tissue are well fostered to reach high cell density. In normal tissue, most cells stay within around 100 μm to blood vessels, because the nutrients are depleted at this distance. This means for active tissues, the capillary network has to be dense enough to balance the consumption during cell metabolism. Similarly, in our micro-bioreactor design, we try to mimic the real nutrient delivery using a dense capillary network. However, due to the theoretical complexity of branching capillary structure, parallel straight capillary system is preferred in this work. Approximately, a real capillary can be regarded as an assembly of many segments of straight capillaries. Therefore we designed and fabricated the micro bioreactor using PμSL as shown in Fig. 4. The capillaries are 800 μm long with 20-μm inner radius and 40-

μm outer radius, the distance between the nearest points of two adjacent parallel tubes is 40 μm. Two ring structures as “artery” and “vein” are connected to the bioreactor chamber which is filled with parallel capillaries. The external nutrient supply will be connected to these two rings which have 400-μm inner diameter. Figure 4(d) shows the cross-section view of a micro-bioreactor. Since the volume of the reactor is only 0.13 μL, it allows culturing about 1,300 cells at the level of 10⁷cells/mL.

In stead of trial and error in culture experiments, we apply numerical method to study the mass transport by a PEG micro-tube which will eventually guide our bioreactor design and cell culture experiment. Without studying the kinetics of tissue growth or cell proliferation, the purpose of this numerical method is to design the right dimensions and density of artificial capillaries, such that all cells in the bioreactor are well nourished even at maximum cell density. Therefore, as a “worst case scenario”, we assume the cell density is at the maximum value which is derived from the average cell size in the case of yeast culture. Coupled with a nutrient consumption model, the simulation will tell the distribution of nutrients in the micro-bioreactor which is full of cells. We have reported the details of the simulation (Xia et al. 2006). Basically, it is a diffusion limited problem with static governing equations:

Table 1 The basic capabilities of our projection micro stereolithography system

Resolution	Speed	Max. sample size
2 μm (in plane or horizontal) 1 μm (off plane or vertical)	4 mm ³ /hour (limited by viscosity of resins)	15 mm × 11 mm × 10 mm

$$D_{pi} \nabla^2 c_i = 0 \quad \text{In capillary wall} \tag{1}$$

$$D_{ii} \nabla^2 c_i - R_i = 0 \quad \text{In cell suspension} \tag{2}$$

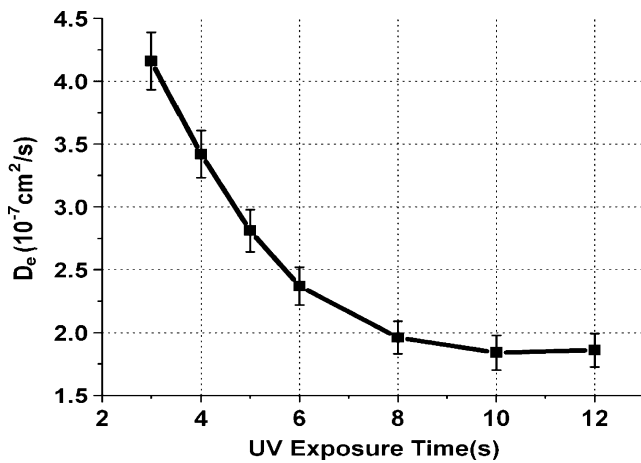
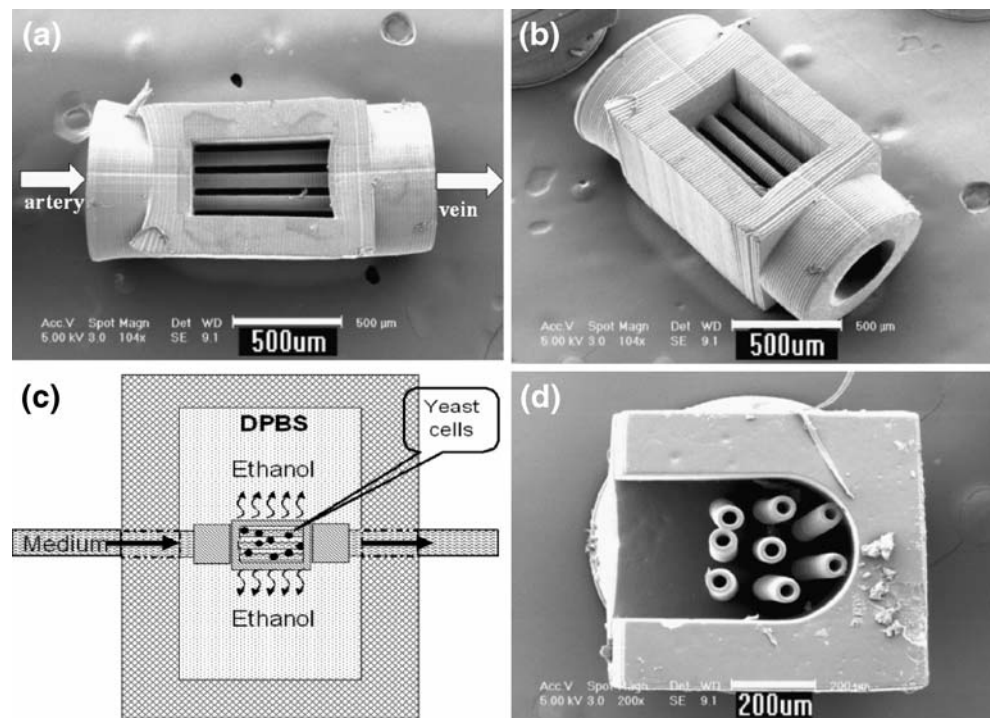


Fig. 3 Experimental data of effective diffusion coefficient of ethanol in 200- μm thick PEG (MW575) films cured using different UV exposure time, temperature=20°C. UV source for film fabrication: wave length=390 nm, intensity=1.1 mW/cm^2

Here D_{pi} , D_{ti} are the diffusion coefficients for metabolite species i in polymer and in tissue respectively, they are assumed to be constant. c_i and R_i are the concentration and consumption rate of species i . In the case of steady state, the process of cells consuming metabolites is often described by Michaelis-Menten kinetics (Michaelis and Menten 1913; Briggs and Haldane 1925):

$$R_i = \frac{V_{\max} c_i}{K_M + c_i} \quad (3)$$

Fig. 4 (a), (b), (d) different views of a micro-bioreactor; (c) yeast cell culture device, the culture medium is pumped from external pipe through the polymer capillaries in the micro-bioreactor. The bioreactor is submerged in DPBS (Dulbecco's Phosphate Buffered Saline) solution. When the culture medium flows through the capillaries, it will diffuse out through the wall of capillaries. The glucose metabolism of yeast cells will produce ethanol which will diffuse into the DPBS solution



Where V_{\max} is the maximal uptake rate and K_M is the metabolite concentration when the uptake rate is half of the maximum. In Michaelis-Menten kinetics, the consumption behavior follows first order kinetics at low concentration. That means the consumption rate is proportional to the concentration. As the concentration of metabolites increases, the consumption behavior will become zero order kinetics gradually. At a certain point, the cell is saturated and the intake of metabolites reaches a plateau.

Yeast cell *Saccharomyces cerevisiae* is well studied of their growth cycles, so we used it as a model to testify the function of our micro-bioreactors. *S. cerevisiae* cell growth has two phases: Glucose is first catabolized fermentatively into carbon dioxide and ethanol (Phase I), and then when the glucose is limited (<830 nmol/mL), ethanol is respired to carbon dioxide and water with the presence of oxygen (Phase II). The biomass production rate in Phase II is much slower than that in Phase I (Otterstedt et al. 2004). Therefore, we can neglect the biomass produced in Phase II. Furthermore, in our experiment we will try to inhibit Phase II metabolism by removing the ethanol. The effective diffusion coefficient of glucose in crosslinked PEG (MW575) is measured using the method mentioned in (Kaufmann and Leonard 1968). The flow rate in the channels is set at 0.5 mm/s . The Michaelis kinetic constants V_{\max} and K_M are from (Otterstedt et al. 2004). The average protein and biomass weight of single *Saccharomyces cerevisiae* yeast are $6 \times 10^{-12} \text{g}$ and $15 \times 10^{-12} \text{g}$ (Sherman and Hicks 1991), respectively. From our scanning electronic microscopy

measurement, the diameter of our cultured *S. cerevisiae* yeast cells (strain INVSc1) is $3.14 \pm 0.61 \mu\text{m}$ (Fig. 5). When the cells are packed together in a most insufficient way which is cells occupy the eight vertices of a cube, then the cell density is $3.2 \times 10^{10}/\text{mL}$. The other simulation parameters are set as follows: $D_{pi}=1.1 \times 10^{-9} \text{ cm}^2/\text{s}$, $D_{ti}=1.1 \times 10^{-6} \text{ cm}^2/\text{s}$ (Vicente et al. 1998), $C_0=110 \mu\text{mol}/\text{mL}$ (concentration of glucose in polymer capillaries), $V_{\text{MAX}}=663 \text{ nmol}/\text{mg protein}/\text{min}$, $K_M=76 \mu\text{mol}/\text{mL}$.

Our simulation indicates that the bottleneck of effective glucose transport is the permeability of polymer capillaries. The glucose concentration drops off more than 95% after diffusing through the capillary wall. The simulation shows that if the center to center distance of the capillaries is set to $120 \mu\text{m}$ and the wall of the capillary is $10 \mu\text{m}$, then the inner radius of the capillary has to be larger than $20 \mu\text{m}$ to ensure that all the yeast cells in the bioreactor has a high enough ($>830 \text{ nmol}/\text{mL}$) glucose concentration to stay in the mixed respiro-fermentative metabolism and produce ethanol (Fig. 5). This configuration corresponds to $80.2 \text{ capillaries}/\text{mm}^2$ if capillaries are in hexagonal arrangement. By increasing the inner radius of the capillary, not only the perfusion of the culture medium is increased, but also the gap between capillaries is decreased. It is equivalent to increase the density of the capillary. When the inner radius is $20 \mu\text{m}$, the lowest glucose concentration in the bioreactor is $880 \text{ nmol}/\text{mL}$. Further decreasing the inner radius of capillaries will decrease the glucose concentration in the bioreactor and force some yeast cells start to consume ethanol (Otterstedt et al. 2004; Verduyn et al. 1984). The biomass growth becomes much slower than at a higher glucose concentration. Two experiments at different points of the simulation curve are also shown in Fig. 5. Experiment A is in the Phase I region that the glucose concentration in the bioreactor is much higher than $830 \text{ nmol}/\text{mL}$. Experiment B is at the cutoff region between Phase I and Phase II. We observed dramatic difference of the biomass production (Fig. 5(b) and (c)). Actually in experiment A (Fig. 5(b)), the yeast cells filled the whole bioreactor and even pushed the cells on top out of the bioreactor during culture. When the bioreactor was removed from the culture chamber, the top layers of yeasts were washed away. However, experiment B (Fig. 5c) shows the exact amount of yeast that we achieved. According to the simulation, in experiment B, the yeast cells should also have fully filled the bioreactor as shown in experiment A. We contribute this error to a low glucose concentration in the bioreactor right after the cell seeding. In experiment B, the capillaries were sparser than that in experiment A. Without cells blocking the way, the glucose diffusing from the capillary quickly escaped from the bioreactor, causing a too low glucose concentration to keep the proliferation of yeast cells. A more detailed model to better capture the real

time growth of yeast cells in bioreactors will be our future efforts.

During the growth of yeast number in the bioreactor, the yeast cells did not consume all the glucose diffusing from the capillaries. Therefore, some glucose leaked from the bioreactor and dissolved in the DPBS solution. As a result, the glucose concentration in the DPBS solution increased. The amount of glucose leaking from the bioreactor depended on how many cells were in the bioreactor. The more cells the less leaking, thus the glucose concentration in the DPBS solution increased slower. Figure 6 shows the average rate of glucose concentration in the DPBS solution in experiment A (Fig. 5(b)). The average rate of glucose concentration is calculated by dividing the difference of glucose concentration by the time between current and last measurements. From Fig. 6, in experiment A, the yeast population in the bioreactor kept increasing during the culture. The glucose rate decreased almost 10 times, but the actual number of yeast increased more than 10,000 times. We attribute this discrepancy to two possible reasons: First, in Michaelis-Menten kinetics, the glucose consumption rate of yeast varies with the local glucose concentration. The increase of yeast population in the bioreactor changed the glucose distribution and thus changed the overall relationship of yeast number and glucose consumption which was not linear. The other reason is that not all the yeast cells were consuming glucose at the end of experiment. The yeasts on top were too far away from the capillary, such that the local glucose concentration was too low for the yeast to do glucose metabolism (Otterstedt et al. 2004).

4 Methods

4.1 Measurement of effective diffusion coefficient of ethanol in PEG membranes

We measured the effective diffusion coefficient of ethanol in PEG membranes using the Kaufmann-Leonard method (Kaufmann and Leonard 1968). Two identical stirred compartments were filled with deionized water and 50 w% ethanol water solution. These two compartments were separated by a $200\text{-}\mu\text{m}$ PEG membrane which was fabricated by UV-polymerizing a layer of PEG diacrylate solution between two glass slices. The motor stirred at a rate of 1 Hz. After 10 min, the concentration of ethanol in deionized water was measured using QED alcohol test kit (OraSure Technologies, Inc.). Since the change of ethanol concentration in both compartments was very small compared to 50 w% ethanol solution, we assumed the diffusion mass flux $= -D_e \times C_0 / d$ was constant during the measurement. Here D_e is the effective diffusion coefficient; C_0 is the concentration of ethanol in 50 w% ethanol

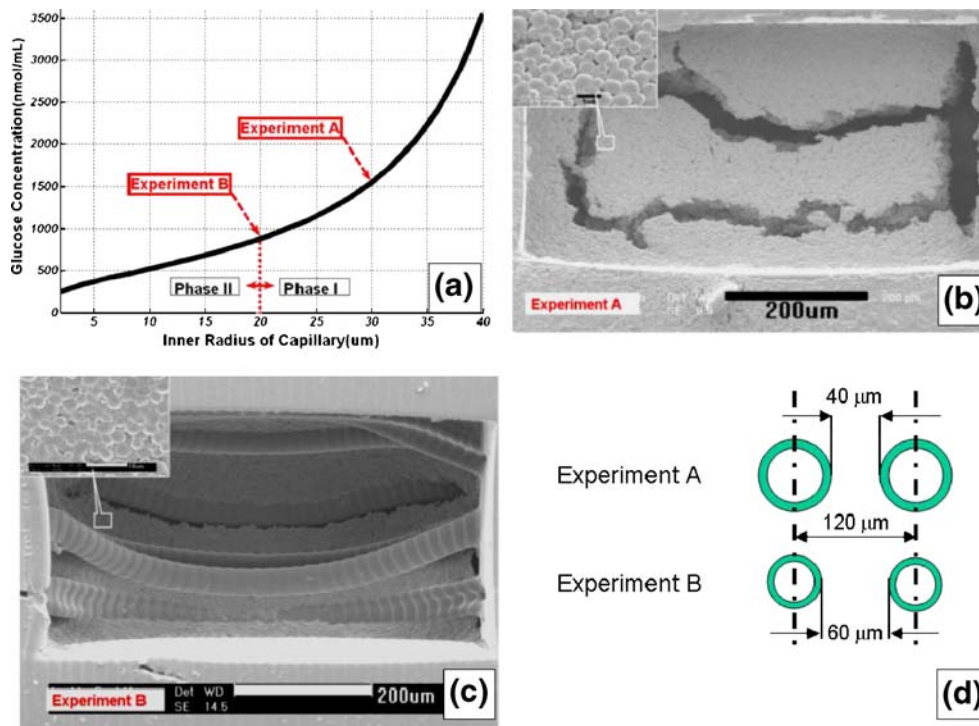


Fig. 5 (a) Simulation results indicating the minimum glucose concentration in a bioreactor increases as the inner radius of capillaries increases. (b), (c) and (d) Two experiments based on yeast model were conducted to verify the simulation. In experiment A, the inner radius of capillaries was 30 μm , the glucose concentration in a bioreactor was within Phase I metabolism of yeast such that the number of yeast

cells grew fast and filled the whole bioreactor. The cracks were due to the collapse of capillaries when the sample was dried in air. In experiment B, the inner radius of the capillary was 20 μm . The glucose concentration in the bioreactor decreased and we saw much less yeast cells in the bioreactor. The center-to-center spacing of capillaries was 120 μm ; the thickness of capillary wall was 10 μm

solution and d is the thickness of PEG membranes. Therefore D_e can be calculated from equation $\delta m = D_e \times C_0 \times \delta t / d$. Here δm is the amount of ethanol in deionized water during a time period of δt .

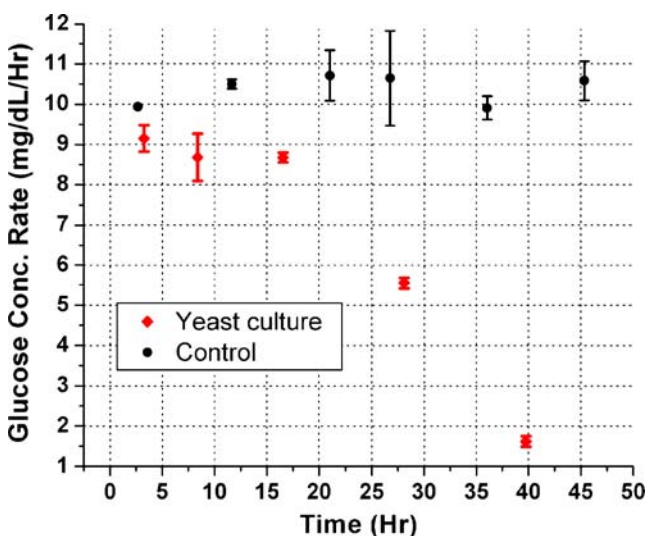


Fig. 6 The average increasing rate of glucose concentration in the DPBS solution

4.2 Yeast cell culture

The yeast we used was diploid strain INVSc1 (Invitrogen). Before yeast culture, the bioreactors were fabricated using $P\mu\text{SL}$ and kept in 100% ethanol for 24 h and biology grade water for 24 h to remove the residue monomer and initiator, also to increase the permeability of the capillaries. The yeast suspension in 1.5 mL microcentrifuge tube was moved from -70°C freezer and left in 20°C room temperature for 20 min before they were seeded in the micro bioreactor using 0.1–10 μL micro pipette. The number of seeded yeast was around 80. The micro bioreactor was placed in the reaction chamber (1 in. \times 0.5 in. \times 0.5 in.) filled with DPBS. Two steel micro tubes with OD 400 μm penetrated the chamber side walls and were connected to the micro bioreactor inside as shown in Fig. 4(c). The chamber was covered with quarter inch thick transparent PLEX sheet to prevent possible contamination. The yeast culture medium YPD (1 g yeast extract (Difco), 2 g Peptone (Difco), 2 g D-glucose, 100 mL distilled water) was delivered at a flow rate of 0.5 mm/s through the capillaries in the micro bioreactor. The culture chamber is kept in a humidified incubator at 30°C for 45 h. The DPBS solution in the chamber was replaced with fresh one every

6–10 h to remove the ethanol in the chamber. The glucose concentration in the replaced DPBS was measured using GlucCell™ glucose monitoring system. Finally, the incubated micro bioreactor was removed from the chamber and dried in air at room temperature for 1 h before sputtering coating and SEM observation.

5 Conclusion

Projection Micro-Stereolithography (PμSL) promises rapid design and manufacturing of advanced micro bioreactors by offering a unique opportunity to culture tissues *in vitro*. By integrating high density micro capillary channels within the micro bioreactors, the mass transport can be enhanced by advection to withstand the increasing demand of oxygen and nutrients during cell growth. Simulation based on glucose diffusion model showed that the bottleneck of effective transport was the diffusivity of the polymer material of the capillary. The glucose concentration dramatically decreased after diffusing through the wall of the capillary. The *S. cerevisiae* yeast cell culture well verified the simulation prediction. Not only is this model applicable for glucose, but also for the transport of other metabolites for different cells. Our simulation modeling can predict how far the nutrients transport into cell layers. With the predicted transport distance, we can precisely control the density of the polymer capillary to ensure that all the cells in the micro bioreactor are in healthy nutrient state.

Acknowledgement This project was supported by the Gauthier Exploratory Research Foundation.

References

- R. Dunn, S. Watson, Why climb a ladder when you can take the elevator? *Plast Reconstr Surg* **107**, 283 (2001)
- G.I. Taylor, J.H. Palmer, The vascular territories (angiosomes) of the body: experimental study and clinical applications. *Br J Plast Surg* **40**, 113–141 (1987)
- Francois Berthiaume and Martin L. Yarmush, *Encyclopedia of Physical Science and Technology*, 3rd edn. (Academic Press, 2002), **16**, p817
- Y.K. Ruben, J.S. Henryk, K. Sales, P. Butler, M.S. Alexander, The roles of tissue engineering and vascularisation in the development of micro-vascular networks: a review. *Biomaterials* **26**, 1857–1875 (2005)
- R.M. Sutherland et al. Oxygenation and differentiation in multicellular spheroids of human colon carcinoma. *Cancer Res.* **46**, 5320–5329 (1986)
- I. Martin et al. Method for quantitative analysis of glycosaminoglycan distribution in cultured natural and engineered cartilage. *Ann. Biomed. Eng.* **27**, 656–662 (1999)
- T. Neumann, B.S. Nicholson, J.E. Sanders, Tissue engineering of perfused microvessels. *Microvasc Res* **66**, 59–67 (2003)
- L.G. Griffith, B. Wu, M.J. Cima, M.J. Powers, B. Chaignaud, J.P. Vacanti, *In vitro* organogenesis of liver tissue. *Ann NY Acad Sci* **831**, 382–97 (1997)
- J.T. Borenstein et al. Microfabrication Technology for Vascularized Tissue Engineering. *BMMD* **4**(3), 167–175 (2002)
- S. Levenberg, J. Rouwkema, M. Macdonald, E.S. Garfein, D.S. Kohane, D.C. Darland, R. Marini, C.A. Van Blitterswijk, R.C. Mulligan, P.A.D. Amore, R. Langer, Engineering vascularized skeletal muscle tissue. *Nat Biotechnol* **23**, 879–884 (2005)
- C. Sun, N. Fang, D.M. Wu, X. Zhang, Projection micro-stereolithography using digital micro-mirror dynamic mask. *Sensors and Actuators A* **121**, 113–120 (2005)
- B.D. Ratner, S.J. Bryant, *Biomaterials: Where We Have Been and Where We Are Going*. *Annu. Rev. Biomed. Eng* **6**, 41–75 (2004)
- Q. Hou, P.A. De Bank, M. Kevin, Shakesheff, Injectable scaffolds for tissue regeneration. *J. Mater. Chem.* **14**, 1915–1923 (2004)
- E. Manias, J. Chen, N. Fang, X. Zhang, Polymeric Micromechanical Components with tunable Stiffness. *Appl Phys Lett* **79**(11), 1700–1702 (2001)
- N. Fang, C. Sun, X. Zhang, Diffusion-limited photopolymerization in scanning micro-stereolithography. *Appl. Phys. A* **79**, 1839–1842 (2004)
- C.G. Xia, C. Sun, D.M. Wu, X. Zhang, N. Fang, 3D Microfabricated Bioreactors. *NSTI-Nanotech* **2**, 140–143 (2006)
- L. Michaelis, M. Menten, Die Kinetik der Invertinwirkung. *Biochem. Z.* **49**, 333–369 (1913)
- G.E. Briggs, J.B.S. Haldane, A note on the kinetics of enzyme action. *Biochem. J.* **19**, 339 (1925)
- K. Otterstedt et al. Switching the mode of metabolism in the yeast *Saccharomyces cerevisiae*. *EMBO reports* **5**(5), 532–537 (2004)
- T.G. Kaufmann, E.F. Leonard, Mechanism of interfacial mass transfer in membrane transport. *AIChE J.* **14**, 421 (1968)
- F. Sherman, J. Hicks, Getting started with yeast. *Methods in Enzymology* **194**, 3–21 (1991)
- A.A. Vicente, M. Dluhy, E.C. Ferreira, M. Mota, J.A. Teixeira, Mass transfer properties of glucose and O₂ in *Saccharomyces cerevisiae* flocs. *Biochem Eng J* **2**, 35–43 (1998)
- C. Verduyn, T.P.L. Zomerdijk, J.P. Van Dijken, W.A. Scheffers, Continuous measurement of ethanol production by aerobic yeast suspension with an enzyme electrode. *Appl Microbiol Biotechnol* **19**, 181–185 (1984)